Advanced RFID-Robot With Rotating Antennas for Smart Inventory in High-Density Shelving Systems

Andrea Motroni, *Member, IEEE*, Salvatore D'Avella, *Member, IEEE*, Alice Buffi, *Senior Member, IEEE*, Paolo Tripicchio, *Senior Member, IEEE*, Matteo Unetti, Glauco Cecchi, *Student Member, IEEE*, and Paolo Nepa, *Senior Member, IEEE*

***Abstract*—This paper presents the development and testing of a robot designed for automated inventory and 3D localization of items in high-density shelving systems. To enhance accuracy in locating UHF-RFID tagged objects by using synthetic aperture-based methods, rotating antennas are installed on the robot. This allows more degrees of freedom in antenna trajectory, by reaching large synthetic apertures that may deliver high-performance localization. The robot can navigate complex environments by utilizing a depth camera and a visual odometry system, and it can effectively avoid obstacles with the help of a Laser Imaging Detection And Ranging system. Extensive testing is conducted in a realistic shop-like scenario where tagged products are placed on either wooden shelves or hung on metal racks. The robot navigation capabilities are verified together with its inventory and localization performance for different visibility conditions of the tagged items.**

***Index Terms*—Autonomous robot, retail robot, UHF-RFID robot, RFID rotating antenna, smart inventory, SLAM, tagged item traceability, tag localization.**

I. Introduction

AUTONOMOUS robots and vehicles are spreading more and more in our working, social, and private lives. Just think about industrial robots working along conveying lines [1], autonomous wheeled vehicles handling goods and pallets, but even small robots performing daily activities such as grass mowing, house cleaning or Ambient Assisted Living [2].

Robots used for inventory operations in logistics belong to the family of autonomous robots. They find applications for the management of items and pallets, both in raw material and finished goods warehouses. Particularly, retail robots also exist to perform inventory and management of items in shops of small to large sizes. Moreover, latest versions consist of robots able to locate items or grasp them, or to work as shopping-assistant in huge malls [3]. They are equipped with several sensors for the navigation system which plays a crucial role.

Robot motion can be pursued thanks to a remote control or an autonomous navigation system. Indeed, robots can be moved in the operating scenario through the knowledge of the map or they can perform Simultaneous Localization and Mapping (SLAM) [4], [5], [6], by acquiring environment information in real-time. For this purpose, several solutions can be adopted. Machine vision is the most commonly utilized technology for autonomous system navigation and object detection [7], [8], [9]. Such approach relies on detecting and identifying peculiar characteristics in the surroundings and yet requires consistent and homogeneous lighting. However, when considering outdoor surroundings or the traversal of different places or facilities, these approaches may suffer from the existence of light interference such as shadows or changing illumination characteristics. Another issue is the object similarity, which makes hard the discrimination among elements of the same type. Because of its versatility and resilience, Laser Imaging Detection And Ranging (LIDAR) is the most promising light detection solution. LIDAR can sense obstacles and walls, thus building accurate maps of the environs, and allowing robot self-localization [10], [11]. It is noteworthy the adoption of wireless systems that leverage many sources of information to reach robot localization. Among them, there are Radio Frequency (RF) systems such as Wi-Fi, Bluetooth, or Radio Frequency IDentification (RFID), ultrasounds, or Ultra Wide Band (UWB) radars [4], [12], [13].

Advanced retail/warehouse robots are also required to perform item inventory with high accuracy. Conventional solutions foresee the adoption of barcodes or QR codes. This leads to the need for an optical reader on the robot side. However, a Line-of-Sight (LOS) condition between the scanner and the label with the printed barcode/QR code is as necessary as difficult to obtain, especially when they are

Manuscript received 20 December 2023; revised 6 February 2024; accepted 20 February 2024. Date of publication 23 February 2024; date of current version 18 June 2024. This work was supported in part by the PARTITALIA Srl within the Project MONITOR (A Cyber Physical System for the Automatic and Real-Time Monitoring of Items in Industrial Scenarios and Large Warehouses) in the Framework of "Fund for Sustainable Growth - "Smart Factory" PON I&C 2014–2020, D.M. 5 March 2018 under Grant CUP B41B20000330005, and in part by the Italian Ministry of University and Research (MUR) in the Framework of both the CrossLab Project (Departments of Excellence) and the FoReLab Project (Departments of Excellence). *(Andrea Motroni and Salvatore D'Avella contributed equally to this work.) (Corresponding author: Andrea Motroni.)*

Andrea Motroni and Glauco Cecchi are with the Department of Information Engineering, University of Pisa, 56122 Pisa, Italy (e-mail: andrea.motroni@unipi.it; glauco.cecchi@phd.unipi.it).

Salvatore D'Avella, Paolo Tripicchio, and Matteo Unetti are with the Department of Excellence in Robotics and AI, Scuola Superiore Sant'Anna, 56127 Pisa, Italy (e-mail: s.davella@santannapisa.it; paolo.tripicchio@santannapisa.it; m.unetti@santannapisa.it).

Alice Buffi is with the Department of Energy, Systems, Territory and Constructions Engineering, University of Pisa, 56122 Pisa, Italy (e-mail: alice.buffi@unipi.it).

Paolo Nepa is with the Department of Information Engineering, University of Pisa, 56122 Pisa, Italy, and also with the Institute of Electronics, Computer and Telecommunication Engineering, Italian National Research Council, 10129 Turin, Italy (e-mail: paolo.nepa@unipi.it).

Digital Object Identifier 10.1109/JRFID.2024.3369470

folded and stacked on shelves or hung on display cabinets. More accurate inventory operations brought to combine RFID technology with retail robots [14]. Indeed, an RFID robot is a well-suitable candidate thanks to the use of radio waves at the Ultra-High-Frequency (UHF) band, which can propagate through obstacles, by guaranteeing identification even in Non-LOS (NLOS) conditions. Essentially, a *UHF-RFID robot* is a robot equipped with a UHF-RFID reader and one or more antennas [15]. Several examples already exist in the literature [12], [16], [17], [18], [19], [20], [21], and in the market too [22]. Their structure has to be suitable for moving in the narrow spaces of a shop or a warehouse, and for sharing space with personnel and customers. Moreover, UHF-RFID robots represent a simpler and scalable solution with respect to the adoption of a large infrastructure of antennas to perform item localization in retail scenarios or in huge warehouses [23].

In this framework, the MONITOR Project aims to develop an advanced UHF-RFID robot able to perform item inventory and localization in high-density shelving scenarios [24], [25]. To guarantee high accuracy in item localization, the principle of the Synthetic Aperture Radar (SAR) is exploited [26], [27]. The main novelty consists in the adoption of UHF-RFID antennas rotating through mechanical arms, as presented in [28] for the first time. Indeed, the combination of the robot motion with the rotating arms, allows the creation of antenna trajectories varying continuously and simultaneously along all the three orthogonal coordinates [25], thus enhancing 3D item localization performance.

In this paper we present and characterize the mobile robotic platform developed within the MONITOR Project. The system presented in [28] is here deeply described with particular attention on the choice of the main parameters for the platform design. Moreover, a detailed description of the navigation system is introduced, which is crucial to perform SAR-based localization. The main robot features and capability are demonstrated in an indoor environment where a shop-like scenario is replicated. Experimental results show the localization performance in finding the 3D position of items equipped with UHF-RFID passive tags, by considering different materials of tagged items and different visibility conditions.

The rest of the paper is organized as follows. Section II presents the RFID-robot platform. Then, Section III describes the navigation system exploiting both the depth camera and the tracking camera. Later on, the SAR-based localization is presented in Section IV with experimental results of inventory and localization, by comparing performance with and without antenna rotation, for different materials of tagged items and variable visibility conditions. Finally, Section V draws the conclusions.

II. The MONITOR Robot With Rotating Antennas

The idea of the MONITOR robot was born to face the issue of high-reliability inventory and localization in retail or warehouse scenarios. To pursue 3D localization of items, we implemented SAR-based localization. The latter requires a relative motion between the reader antenna and the tagged items, and this can be pursued thanks to the robot that creates a *synthetic-array* through its trajectory. RFID reader antennas can move on a plane parallel to the floor thus creating a linear or a planar synthetic array, if the robot trajectory is rectilinear or curvilinear, respectively. However, accurate 3D localization relies on the length of the synthetic arrays, i.e., *synthetic aperture*, in all three orthogonal directions. The larger the aperture, the better the localization performance. This reflects the need for an antenna motion along a 3D trajectory. Hence the idea of installing an antenna handling-system on the robot to increase degree-of-freedoms of its trajectory. A first solution could be the realization of a vertical handling for the antenna [29]. If the robot moves along a curvilinear trajectory, the combination with a vertical shift allows getting a 3D antenna trajectory. However, by considering the small width of aisles, typical of retail/warehouse scenarios, we conceived a solution that guarantees a 3D antenna trajectory even for rectilinear robot trajectory. Hence the idea of a robot with rotating antennas.

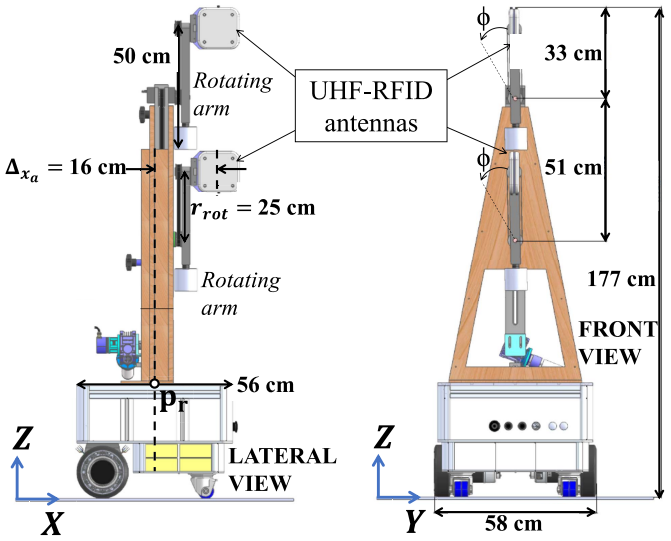

Fig. 1. CAD sketch of the UHF-RFID robot developed within the MONITOR Project with UHF-RFID rotating antennas.

A. Rotating Antennas

Several mechanical solutions could be adopted to get antenna rotation on the robot. Here, we considered the adoption of a couple of rotating arms as a good compromise between mechanical-implementation complexity and localization accuracy. Fig. 1 shows the CAD design of the MONITOR robot. Two arms consisting of devices with pulleys and transmission belts are installed above the mobile platform at different heights. Each arm rotates two antennas that are installed back to back, to guarantee tag detection at both sides of the robot. While rotating the antenna, the mechanism keeps it orthogonal to the ground, by ensuring the antenna maximum radiation in lateral directions. The upper and lower antennas rotate synchronously, just to simplify the mechanical system.

The mechanical arms allow to create the antenna rotation on the plane orthogonal with respect to that of the robot direction. The combination of robot motion and arm rotation creates a

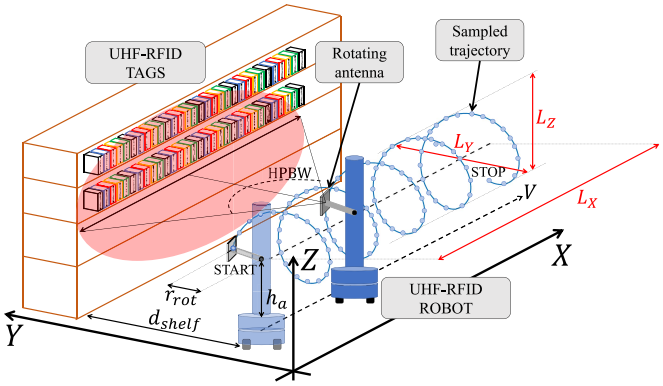

Fig. 2. Scenario of the MONITOR Project: the RFID-Robot with rotating antennas performs straight trajectories along the *X*-axis parallel to the shelf. Antennas rotate on the *YZ*-plane orthogonal to the motion direction by providing a 3D synthetic array.

3D trajectory of the reader antennas, which assume a helicoid shape, as exemplified in Fig. 2 for a single antenna. Generally, the mobile robot base is not constrained to follow rectilinear trajectories, by enhancing the system versatility.

It is noteworthy that the adoption of rotating antennas on robots was also proposed in [21] to perform Rotating SAR (RoSAR) localization. However, the small omnidirectional antenna was placed on a rotating platform by creating a planar trajectory parallel to the floor, rather than a whole 3D trajectory as proposed in this paper.

Antennas at different heights guarantee the tag detection and localization at several shelving compartments. The vertical distance between antennas has to be selected on the basis of their Half Power Beam Width (HPBW) on the vertical plane. The variation of the antenna footprint on the shelf during rotation is exemplified in Fig. 3 for the upper left antenna.

The main geometrical parameters of the robotic platform have to be selected as a compromise between the encumbrance and the creation of large-enough synthetic arrays, by accounting for the shelf height, the available space and the carrier wavelength λ [24], which is around 30 cm for UHF-RFID systems. The maximum extent of the rotating arm and therefore its rotation radius has been chosen to be shorter than half of the robot base W_R. This avoids hitting goods during inventory rounds. The synthetic-array aperture along the *X*-axis, i.e., L_X, is basically determined by the robot trajectory along that axis (Fig. 2). The synthetic-array apertures along the *Y*-axis, i.e., L_Y, and *Z*-axis, i.e., L_Z, both depend on the radius of the rotation arm r_{rot} and the range of the rotation angle ϕ. For a full revolution of the arm, i.e., $\phi = [0, 2\pi]$ rad, $L_Y = L_Z = 2r_{rot}$. Such lengths of the synthetic arrays have to be intended as maximum possible apertures. Indeed, during the inventory operation, the actual lengths can vary from tag to tag depending on its position on the shelf with respect to the robot trajectory. Based on previous experimental characterization [27], both the synthetic-array aperture should be at least half a meter, whereas the antenna-tag distance should be in the order of few meters.

Another important aspect is the spatial sampling which is related to the read rate achievable with the EPC Global C1G2 protocol. Indeed, it is required to receive

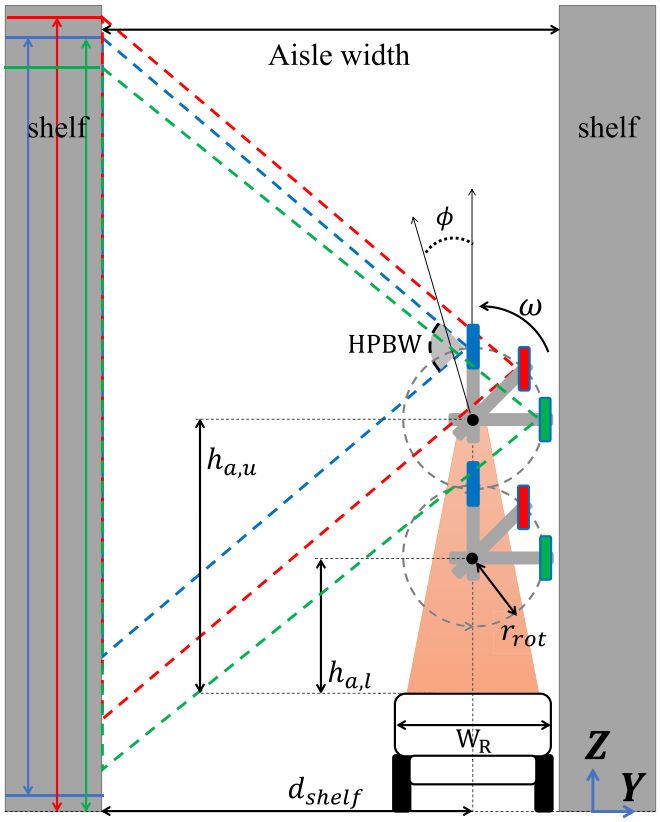

Fig. 3. Lateral view of the UHF-RFID robot with rotating antennas moving between two shelves. The HPBW footprint on the shelf is highlighted for different positions of the upper left antenna during its rotation.

replies from a single tag with an average spatial sampling below $\lambda/[4\sin(\text{HPBW})]$ [27], calculated along the curvilinear abscissa of the antenna trajectory. Since both the robot speed V and the arm-rotation angular speed ω influence the sampling of the tag backscattered signal, they have to be properly chosen by considering the reader interrogation rate.

The antenna positions at each timestamp are calculated by considering the mobile base position and the rotation angle of the mechanical arms. The majority of commercial mobile platforms rely on proprietary solutions for the navigation and localization of the robot. Lately, several RFID-robot manufacturers are following the research trend in robotics and they are providing an open-source implementation of the navigation facilities usually based on the Robot Operating System (ROS) framework [30], [31]. Few products provide analogous functionalities with a different programming interface like Java. Independently on the software modules, commercial robots usually rely on a combination of LIDAR, ultrasound sensors, and wheel encoders to efficiently solve robot navigation and localization issues.

B. The Robot Proof-of-Concept

Fig. 4 shows the Proof-of-Concept of the MONITOR robot with two rotating mechanical arms. The robot base measures $W_R = 0.58$ m (Fig. 3) and it is configured to move with a speed of $V = 10$ cm/s. The arm rotation radius is $r_{rot} = 0.25$ m, and the angular speed is $\omega = 0.48$ rad/s. So, a complete arm revolution lasts 13 s.

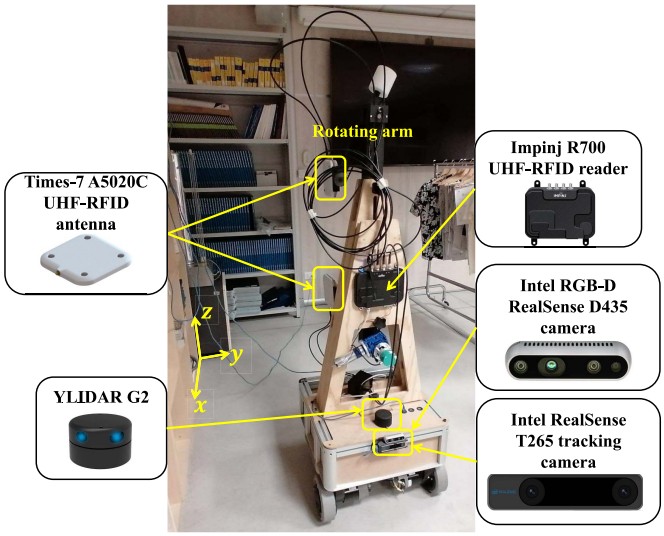

Fig. 4. Proof-of-concept of the MONITOR UHF-RFID robot with UHF-RFID reader and antennas, RGB-D camera, tracking camera, and LIDAR.

The adopted antennas are Times-7 A5020C circularly polarized antennas with a Gain of 5.5 dBiC and a HPBW of 105°. They are controlled by the Impinj R700 reader working at the ETSI (European Telecommunications Standards Institute) RFID frequency band (865-868 MHz). The interrogation period is nearly 10 ms, so guaranteeing the right spatial sampling for the selected values of V and ω.

During experiments, when arm rotation is not enabled, i.e., *fixed antennas* test-case, upper antennas #1 and #3 are at a fixed height of $z = 1.45$ m, while the lower antennas #2 and #4 are at $z = 0.94$ m. When rotation is enabled, i.e., *rotating antennas* test-case, upper antennas change their heights from $z = 1.37$ m to $z = 1.87$ m, whereas lower antennas move from $z = 0.86$ m to $z = 1.36$ m.

The mobile robot is equipped with two different camera sensors and wheel encoders. The information on wheel motion and visual odometry is fused in the Real-Time Appearance-Based Mapping (RTABMap) framework [32]. The first one is the RGB-Depth (RGB-D) camera by Intel, model RealSense D435i, which is used to populate the environment map in 3D and to reconstruct the robot motion. The second camera is an Intel RealSense T265 tracking camera that can provide a visual odometry estimation on its own with a custom hardware-accelerated algorithm running within the camera. The localization error of the T265 camera is 2% on closed paths as reported by the manufacturer. This has been used as a base estimation to improve the localization performance of the SLAM algorithm. Finally, the robot is equipped with a LiDAR sensor for obstacle avoidance, i.e., the model YDLIDAR G2. Cameras and lidars are cost-effective options, making them well-suited for the development of an affordable yet reliable solution.

III. Navigation System

The adopted robotic platform (Fig. 4) uses differential wheel kinematics, meaning that the velocity of each wheel can be adjusted, and the robot may rotate around a point sitting along the shared left and right wheel-axis in order to accomplish a rolling motion. This is known as the Instantaneous Center of Curvature (ICC).

We assume the robot is at the 2D position $[x_r, y_r]^T$, headed in a direction making an angle θ_r with the X-world axis (room reference frame). V_r and V_l are the right and left wheel velocities along the ground. l is the distance between the centers of the two wheels and R is the signed distance from the ICC to the midpoint between the wheels. The ICC can be defined as

$$ICC = \left[x_r - R\,sin(\theta_r), y_r + R\,cos(\theta_r)\right], \tag{1}$$

and R can be solved at any instant as $0.5(V_r + V_l)/(V_r - V_l)$. At time $t + \delta t$ the robot pose can be obtained from

$$\begin{bmatrix} \dot{x_r} \\ \dot{y_r} \\ \dot{\theta_r} \end{bmatrix} = \begin{bmatrix} cos(\omega\delta t) & -sin(\omega\delta t) & 0 \\ sin(\omega\delta t) & cos(\omega\delta t) & 0 \\ 0 & 0 & 1 \end{bmatrix} \begin{bmatrix} x_r - ICC_x \\ y_r - ICC_y \\ \theta_r \end{bmatrix} + \begin{bmatrix} ICC_x \\ ICC_y \\ \omega\delta t \end{bmatrix}, \tag{2}$$

where ω is the angular velocity given by $(V_r - V_l)/l$. It has to be noticed that if the wheels velocities are equal, i.e., $V_r = V_l$, the robot follows a rectilinear trajectory, namely $\omega = 0$ and $R = \infty$. Instead, if $V_r = -V_l$, the robot will undergo an in-place rotation about the midpoint of the wheel axis, i.e., $R = 0$.

For navigation to work, it is important to have a map of the environment, and the process of creating a map is called *mapping*. The RTABMap [32] is a graph SLAM algorithm based on an incremental appearance-based loop closure detector. It employs visual odometry [33] over a Red-Green-Blue (RGB) stream and 3D information from a depth sensor. In our case, the use of a RealSense RGB-D camera allows us to provide both inputs to the algorithm. Visual odometry starts by extracting *Scale-Invariant Feature Transform* (SIFT) and *Speeded Up Robust Feature* (SURF) features from images, and thanks to the depth map of the corresponding scene, the features are correctly placed in the 3D environment and a trajectory is computed, i.e., RTABOdom trajectory. The auxiliary T265 tracking camera provides a robust odometry base speeding up the visual odometry computation and thus leveraging the mobile robot CPU. The loop closure detector uses a bag-of-words approach to determine if a new image is likely to come from an already-known place or a new one. When a loop closure hypothesis is accepted, a new constraint is added to the map graph, and the committed errors in the mapping are minimized by using a graph optimizer. Concurrently, the loop closure updates are used to optimize the final computed trajectory, i.e., RTABPose trajectory.

Once obtained the map, the robot navigates in the environment by using the Adaptive Monte Carlo Localization (AMCL) approach [34]. It is a probabilistic localization system for a moving robot in 2D space that uses a particle filter to track a robot pose against a known map. Given a map of the environment, the algorithm predicts the robot attitude as it moves and perceives its surroundings. It displays the distribution of likely states using a particle filter, where each particle represents a possible state that is a hypothesis about the robot location.

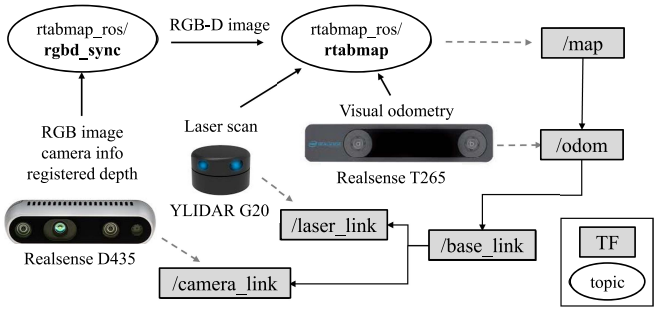

Fig. 5. Sensor input to the RTABMap pipeline and corresponding transforms tree (TF) within the ROS framework.

Fig. 5 shows the employed sensor input for the SLAM algorithm and the synchronization among components in the ROS framework together with the transform tree generated by the software pipeline.

A. Navigation Performance

During the experimental session, the motion of the mobile robot was reconstructed with the SLAM pipeline described above, and Fig. 6 shows the point cloud of the acquired map of the testing environment and an example of the estimated robot motion within it. The map has been computed in real-time contextually to the experimental acquisition.

In [32] an evaluation of the performance of the algorithms employing state-of-the-art benchmarking datasets like KITTI, EuRoc, and TUM has been presented. The metric used for the trajectory accuracy is the absolute trajectory root-mean-square error (ATE), derived from the TUM RGB-D benchmark [35]. The obtained average translation error (in percent) is reported as 1.26%. Thanks to the integration of the T265 odometry into the RTABMap pipeline, the proposed system can reduce the translation error to 1%, which is consistent with the result shown in [32]. For a better understanding, Fig. 7 shows the X and Y coordinates of the trajectories performed by the mobile platform during the test of Fig. 6, as estimated by the T265 tracking camera, the RTABMap Odometry computation (RTABOdom), and the RTABMap Pose estimation (RTABPose).

IV. SAR-Based Localization

For the sake of completeness, the description of the SAR-based localization method named SARFID is here reported. SARFID has been proven to be effective in several scenarios [12], [18], [36]. This mathematical formulation is valid for both the case of a static or a rotating antenna, when it is mounted on a mobile platform. Indeed, we will compare localization performance by adopting fixed antennas with respect to the case of rotating antennas.

From the knowledge of the robot trajectory, the antenna position over time can be easily derived. The estimation of the robot pose at the n-th timestamp can be interpreted in Cartesian coordinates as $\mathbf{p}_{r_n} = [x_{r_n}, y_{r_n}, z_{r_n}]^T$. Consequently, the antenna position can be derived as

$$\mathbf{p}_n = \mathbf{p}_{r_n} + \Delta_n, \tag{3}$$

where $\Delta_n = [\Delta_{x_n}, \Delta_{y_n}, \Delta_{z_n}]^T$ is the antenna offset with respect to the robot base-center, by considering both the orientation of the robot around Z-axis, i.e., $\mathbf{R}_{\theta_n}$, and the antenna rotation of an angle ϕ around the arm rotational joints, i.e., local robot x-axis, $\mathbf{R}_{\phi_n}$, computed as

$$\Delta_n = \mathbf{R}_{\theta_n}\mathbf{R}_{\phi_n}\begin{bmatrix}\Delta_{x_a}\\0\\r_{rot}\end{bmatrix} + \begin{bmatrix}0\\0\\h_a\end{bmatrix}, \tag{4}$$

where h_a is the height of the antenna rotational joint with respect to the robot-base height (Fig. 3) and Δ_{x_a} is the antenna displacement along the local robot x-axis (Fig. 1). By referring to Fig. 3, $h_{a,l} = 0.51$ m for lower antennas, $h_{a,u} = 1.02$ m for upper antennas, and $\Delta_{x_a} = 0.16$ m.

The instantaneous distance between the antenna detecting a tag, being it fixed or rotating, and the tag itself can be written as

$$r_n = \|\mathbf{p}_n - \mathbf{p}_{tag}\|, \tag{5}$$

where $\mathbf{p}_{tag} = [x_{tag}, y_{tag}, z_{tag}]^T$ is the actual tag position.

The received phase of the tag backscattered signal can be written as [27]

$$\varphi_n = -4\pi\frac{r_n}{\lambda} + \varphi_0, \tag{6}$$

where φ_0 is the phase offset that mainly depends on the reader and tag internal circuitry. To release from a calibration procedure, we consider the first phase sample as a reference, i.e., n=1,

$$\Delta\varphi_n = \varphi_n - \varphi_1 = -4\pi\frac{(r_n - r_1)}{\lambda}. \tag{7}$$

Using differential phase shift allows to neglect the phase offset for readings collected within the antenna main beam, where it can be assumed as constant. A phasor notation is adopted to manage the 2π-ambiguity, so avoiding unwrapping techniques [19]. Along the robot trajectory, a set of N_r samples are collected and the resulting normalized phasor sequence can be written as

$$\mathbf{s}(\mathbf{p}_{tag}) = \left[1, e^{j\Delta\varphi_2}, \ldots, e^{j\Delta\varphi_{N_r}}\right]^T. \tag{8}$$

Since the reader-antenna trajectory $\mathbf{p}_n$ is known from the robot navigation system described in Section III, by supposing a hypothetical tag 3D position $\mathbf{p}'_{tag} = [x'_{tag}, y'_{tag}, z'_{tag}]^T$, a hypothetical phasor sequence can be derived according to (8)

$$\mathbf{a}\left(\mathbf{p}'_{tag}\right) = \left[1, e^{j\Delta\varphi'_2}, \ldots, e^{j\Delta\varphi'_{N_r}}\right]^T. \tag{9}$$

Finally, the matching between $\mathbf{s}(\mathbf{p}_{tag})$ and $\mathbf{a}(\mathbf{p}'_{tag})$ is evaluated through the normalized cross-correlation function

$$C\left(\mathbf{p}'_{tag}\right) = \frac{\left|\mathbf{a}^H\left(\mathbf{p}'_{tag}\right)\mathbf{s}(\mathbf{p}_{tag})\right|^2}{\left|\left|\mathbf{a}^H\left(\mathbf{p}'_{tag}\right)\right|\right|^2 \cdot \left|\left|\mathbf{s}(\mathbf{p}_{tag})\right|\right|^2}. \tag{10}$$

The spatial coordinates corresponding to the peak of the cross-correlation function (10) are assumed as the estimated tag position $\hat{\mathbf{p}}_{tag} = [\hat{x}_{tag}, \hat{y}_{tag}, \hat{z}_{tag}]^T$

$$\hat{\mathbf{p}}_{tag} = \arg\max_{\mathbf{p}'_{tag}} C\left(\mathbf{p}'_{tag}\right). \tag{11}$$

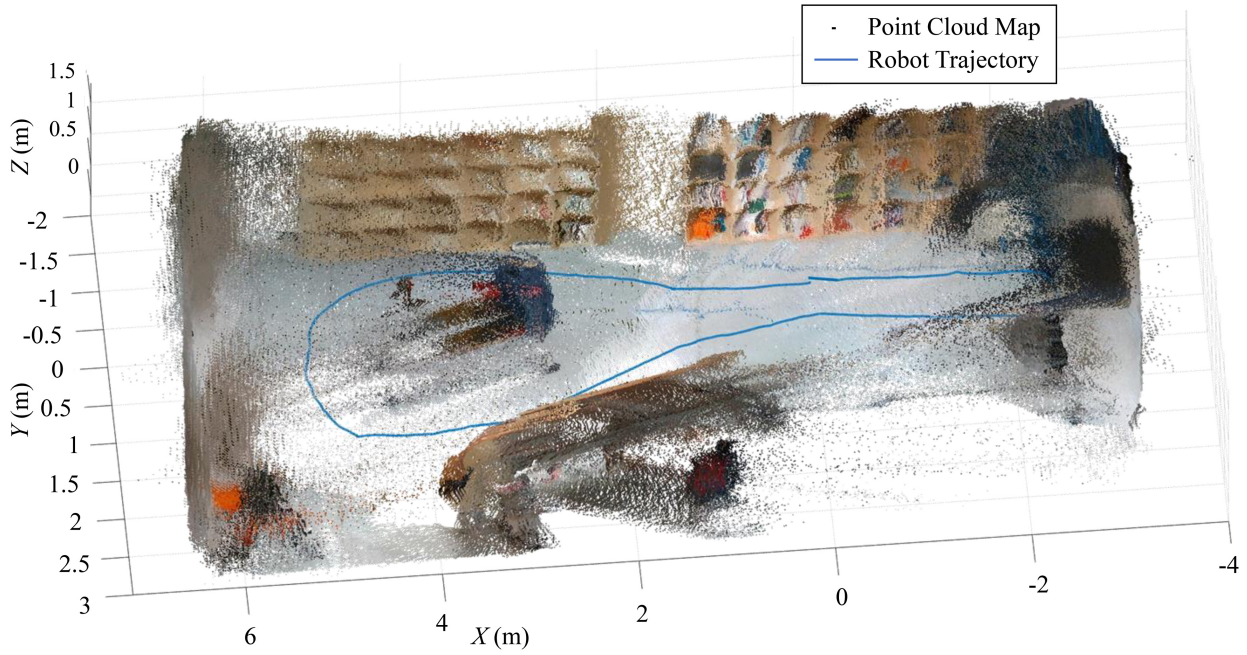

Fig. 6. Point Cloud of the environment as generated by the SLAM pipeline and reconstructed trajectory of the mobile base (RTABPose).

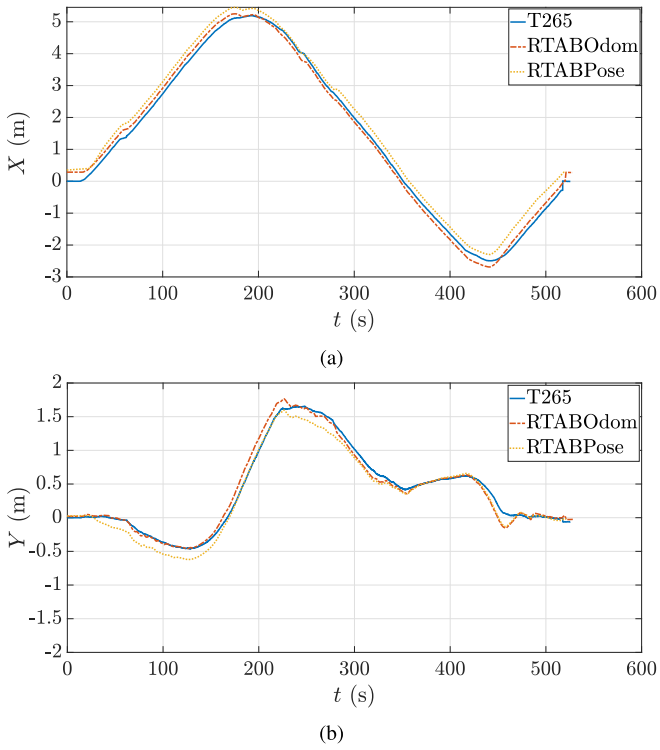

Fig. 7. Coordinates of the trajectory versus time estimated by the T265 camera (T265), the RTABMap Odometry computation (RTABOdom), and RTABMap Pose estimation (RTABPose): (a) X-coordinate and (b) Y-coordinate. They are referred to the test of Fig. 6.

The higher the peak value, the greater the similarity between the normalized phasor sequence and the nominal one. The peak search in (11) can be evaluated through several optimization algorithms. To reduce the computational time, we adopted a Particle Swarm Optimization (PSO) [36] after a first search with a coarse-grained grid [17], by also considering

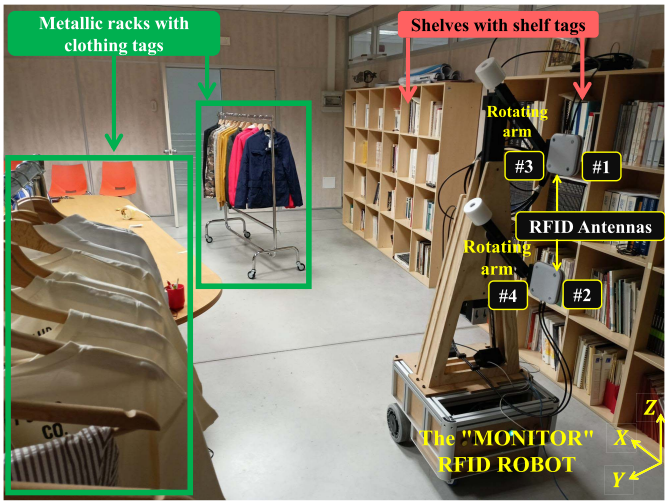

Fig. 8. Experimental shop-like setup realized at the *PERCRO Laboratory* of the IIM of the Scuola Superiore Sant'Anna, Pisa.

the antenna HPBW and the maximum reading range of the tag as stated in the tag datasheet. Indeed, in 3D localization, a grid-search approach with a small resolution would lead to the evaluation of the cross-correlation in a large space volume with a consequent high computational cost.

A. Experimental Setup

Fig. 8 represents the measurement setup realized at the *PERCRO (PERCeptual RObotics) Laboratory* of the *Institute of Mechanical Intelligence (IIM)* of the Scuola Superiore Sant'Anna, Pisa. The room sizes are about 9 m × 5 m. To emulate a shop-like scenario we deployed high-density tags on shelves and racks, by attaching them to card-boxes and clothing labels, respectively. So, the system localization capability can be tested under demanding operating conditions

with a high level of interference due to clutter and mutual coupling among tags. Furthermore, we can verify the effect on the localization performance of the material the tag is attached to, but also the effect of the tag visibility conditions, i.e., LOS with respect to NLOS conditions.

Three measurements setups were built, named as Setup A, B, and C. In Setup A, we deployed a group of 210 commercial *Partitalia LB012* tags attached to card boxes placed in the wooden shelving at the side of the room (Fig. 8), i.e., *shelf tags*. The tag chip is the NXP-U8. Tags are in LOS with random orientation and their heights span from 0.91 m to 1.58 m. In Setup B, metallic racks with clothes are placed in the middle of the room. Clothing labels are tagged with tags of the above-mentioned model, i.e., *clothing tags*. We deployed, a total of 210 clothing tags with random orientation, which can be in LOS or NLOS conditions with respect to the robot position. Before the experiments with above settings, we measured the location of 30 shelf tags and 30 clothing tags by exploiting a laser meter with a ± 2 mm manufacturer measurement accuracy to get a suitable ground truth for evaluating the localization method. For these tags, i.e., *target tags*, we are able to evaluate the localization error, and therefore they were used as targets for the SARFID method to estimate the localization performance. So, the Setup C consists of the group of 30 shelf tags and 30 clothing tags with ground-truth location measurements. Among target tags, shelf tags are selected with an average 43-cm spacing along the X-direction and they are vertically oriented, whereas clothing tags are spaced lower than $\lambda/4$ and randomly oriented. One possible application of this scenario falls in the case where we want to localize only one category of items, e.g., t-shirts instead of trousers. Target tags can be easily searched thanks to the specific Electronic Product Code (EPC). For each setup, the robot runs three complete closed trajectories around the room with fixed antennas and three with rotating antennas. The inventory rounds have been executed with nearby the same duration and robot speed. Inventory performance was validated through experiments with Setup A and Setup B, while localization performance were tested in all the three setups A, B, and C. Table I sums up the features of the three setups.

B. Inventory Performance

Inventory performance with both fixed and rotating antennas is summarized in Table II for Setup A and Setup B, which includes key metrics such as the number of detected tags (percentage of detected tags), total readings, readings per tag, test duration, and the reading rate. Clothing tags and shelf tags are distinguished.

In all tests involving shelf tags (Setup A), 209 out of 210 tags were detected, accounting for 99.52% of the total. In the tests with clothing tags (Setup B), all 210 tags (100%) were successfully detected in each complete trajectory of the robot in the room. Two significant insights can be inferred from these observations. The first one is that, in all test-cases, rotating antennas reach the same percentage of detected tags being the inventory times nearby equal, and consistently deliver higher reading rates due to the additional degrees of freedom in the antenna motion, that improve the probability of tag detection. This also allows us to acquire more phase samples to be used in the SARFID localization method. The second insight is that the MONITOR robot is highly reliable even in the inventory of tagged clothing that are in NLOS. Indeed, a mobile robot with rotating UHF-RFID antennas proves to be a robust solution for RFID tag inventory, as the relative movement between the reader antenna and the tags enhances individual tag detection.

C. Tag Localization Performance

To first deal with the improvements achieved with rotating antennas in localization, a single test-case is analyzed. Fig. 9 shows antenna trajectories for the case of fixed antennas (Fig. 9a) and rotating antennas (Fig. 9b) when detecting a shelf tag placed at $\mathbf{p}_{tag} = [-1.24, -0.88, 1.35]^T$ m as measured by the laser meter (black asterisk marker). We define the synthetic apertures along each axis, $L_X = |\max(x_n) - \min(x_n)|$, $L_Y = |\max(y_n) - \min(y_n)|$, and $L_Z = |\max(z_n) - \min(z_n)|$ as the antenna motion ranges along the X-, Y-, and Z-axis, respectively, during tag detection.

When antennas are fixed (Fig. 9a), the antenna detects the target tag from location $[-0.09, 0.89, 1.45]^T$ m to $[-2.94, 1.23, 1.45]^T$ m. The number of readings is $N_r = 76$ for an average spatial sampling of 4.1 cm. Synthetic apertures along single axes are $[L_X, L_Y, L_Z]^T = [2.87, 0.67, 0]^T$ m. When antennas are rotating (Fig. 9b), the antenna detects the target tag from location $[-1.47, 0.30, 1.22]^T$ m to $[-0.50, 0.17, 1.29]^T$ m. The number of readings is $N_r = 172$ for an average spatial sampling of 5.5 cm. Synthetic apertures along single axes are $[L_X, L_Y, L_Z]^T = [2.60, 1.00, 0.50]^T$ m. As expected, rotating antennas enable larger synthetic arrays along Y- and Z-directions and a greater number of tag readings with respect to fixed antennas. The measured phase in the case of rotating antennas is reported in Fig. 10 compared to the theoretical one related to the sample test-case of Fig. 9b. It can be seen a good agreement between theoretical model and measured data by highlighting the robustness of phase-measurements to the multipath propagation phenomena.

Matching functions along X-, Y-, and Z-axis are represented in Fig. 11a, Fig. 11b, and Fig. 11c, respectively. We compare the performance of fixed antennas (red solid line) and rotating antennas (blue dashed line). It is observable that rotating antennas configuration leads to a narrower main-lobe with respect to fixed antennas configuration, and therefore a better localization performance is expected. This effect is greatly noticeable along the Z–direction, where the fixed antenna exhibits a null span and an ambiguous lobe appears by compromising the Z-coordinate estimation. By naming the localization error vector as the difference between the estimated tag position and the ground truth position, it can be written as $\boldsymbol{\varepsilon} = [\varepsilon_x, \varepsilon_y, \varepsilon_z]^T = [\hat{x}_{tag} - \tilde{x}_{tag}, \hat{y}_{tag} - \tilde{y}_{tag}, \hat{z}_{tag} - \tilde{z}_{tag}]^T$. The Euclidean norm of the error vector $\varepsilon_d = \|\boldsymbol{\varepsilon}\|_2$ represents an aggregated metric to evaluate the localization performance along all the space axes. The resulting estimated tag location is $\hat{\mathbf{p}}_{tag} = [\hat{x}_{tag}, \hat{y}_{tag}, \hat{z}_{tag}]^T = [-1.20, -0.85, 0.64]^T$ m by using fixed antennas, leading to an error of $\varepsilon_d = 71.2$ cm.

TABLE I
NUMBER, POSITION, SPACING AND ORIENTATIONS OF THE RFID TAGS DEPLOYED IN THE THREE SETUPS

	Shelf tags	**Clothing tags**	**Tag Spacing**	**Tag Orientations**
Setup A	210	None	$< \lambda/4$	Random
Setup B	None	210	$< \lambda/4$	Random
Setup C	30	30	43 cm for shelf tags, $< \lambda/4$ for clothing tags	Vertical for shelf tags, random for clothing tags

TABLE II
INVENTORY PERFORMANCE FOR SETUPS A AND B WITH BOTH FIXED AND ROTATING ANTENNAS

	Fixed antennas		**Rotating antennas**	
	Shelves (Setup A)	**Clothes** (Setup B)	**Shelves** (Setup A)	**Clothes** (Setup B)
Shelf tags	209/210 (99.52%)	-	209/210 (99.52%)	-
Clothing Tags	-	210/210 (100%)	-	210/210 (100%)
# total readings	36814	46052	36477	52116
# readings per tag	177	219	174	248
Test time [s]	277	267	259	238
Readings rate [tags/s]	132	172	140	218

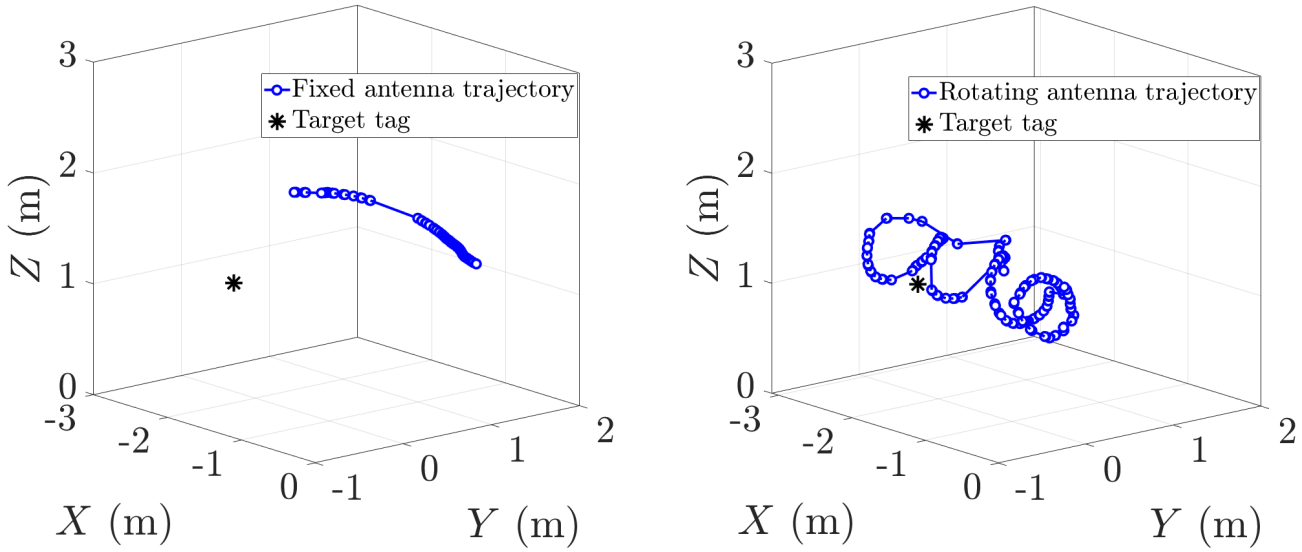

(a) (b)

Fig. 9. Antenna trajectory when detecting a tag placed at $\mathbf{p}_{tag} = [-1.24, -0.88, 1.35]^T$ m in a sample test-case with a) fixed antennas; b) rotating antennas. Antenna trajectory is represented with blue circular markers, and tag location is highlighted with a black asterisk marker.

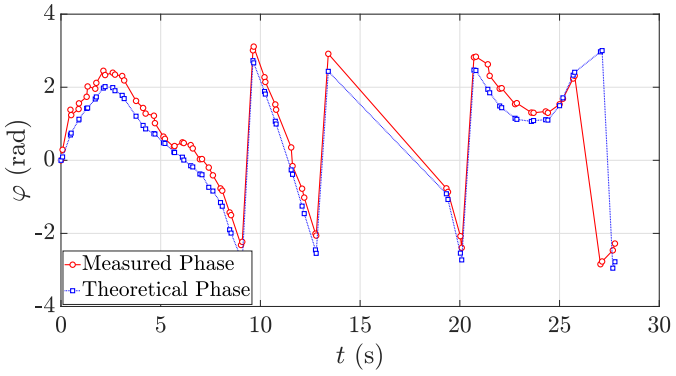

Fig. 10. Measured phase (red circular markers) vs. theoretical one (blue squared markers) related to the sample test-case of Fig. 9b with rotating antennas.

With the rotating antenna, the estimated tag position is $\hat{\mathbf{p}}_{tag} = [\hat{x}_{tag}, \hat{y}_{tag}, \hat{z}_{tag}]^T = [-1.23, -0.88, 1.34]^T$ m, which gives an error of $\varepsilon_d = 1.4$ cm.

D. Performance Comparison: Shelf Tags vs. Clothing Tags

We examined the impact of tag material on localization performance, but also of the tag visibility condition, e.g., LOS, and NLOS. For each measurement setup we performed several experiments, namely we acquired data during consecutive rounds of the robot in the room. Then, we aggregated data in four datasets. The first is related to readings of 218 shelf tags detected by fixed antennas on the robot, i.e., *FA, shelves*, the second refers to data of 135 clothing tags inventoried by fixed antennas, i.e., *FA, clothes*, the third deals with 394 shelf tags read by rotating antennas, i.e., *RA, shelves* and the last one consists of 171 clothing tags detected by rotating antennas, i.e., *RA, clothes*. The boxplot of the 3D localization errors is depicted in Fig. 12 for the four datasets. When considering shelf tags, a mean localization error of 27 cm and 24 cm is obtained for fixed and rotating antennas, respectively. Instead, by analyzing clothing tags, a mean localization error of 42 cm and 15 cm is obtained for fixed and rotating antennas, respectively. Noticeably, antenna rotation decreases localization error

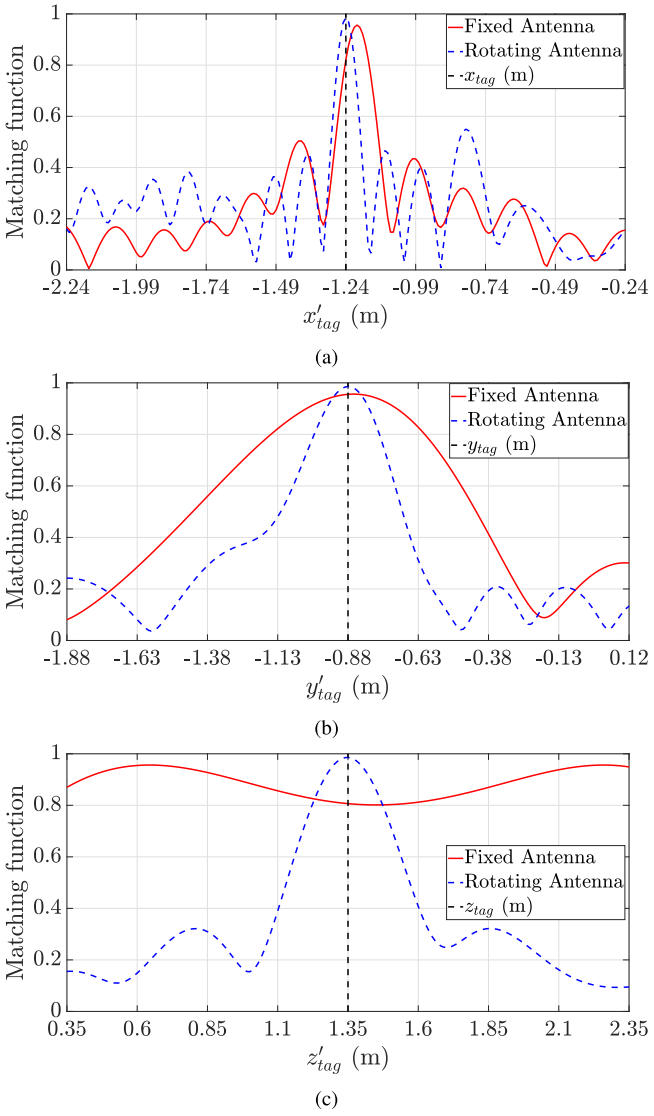

Fig. 11. Cross-correlation functions for the sample test-case represented in Fig. 9 for fixed- antenna (solid red line) and rotating-antenna configuration (dashed blue line) along (a) *X*-axis; (b), *Y*-axis, and (c) *Z*-axis.

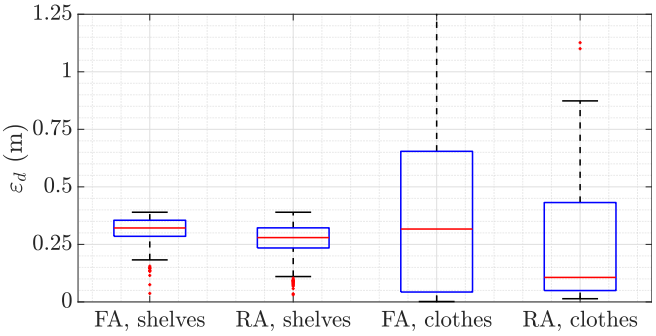

Fig. 12. Boxplot of the 3D localization error on shelf tags detected by fixed antennas, i.e., *FA, shelves*, shelf tags detected by rotating antennas, i.e., *RA, shelves*, clothing tags detected by fixed Antennas, i.e., *FA, clothes*, and clothing tags detected by rotating antennas, i.e., *RA, clothes*.

and its advantage is more apparent during the localization of clothing tags, which often are in NLOS conditions.

Nevertheless, it can be observed that the error deviation is higher for clothing tags, for both fixed and rotating-antennas

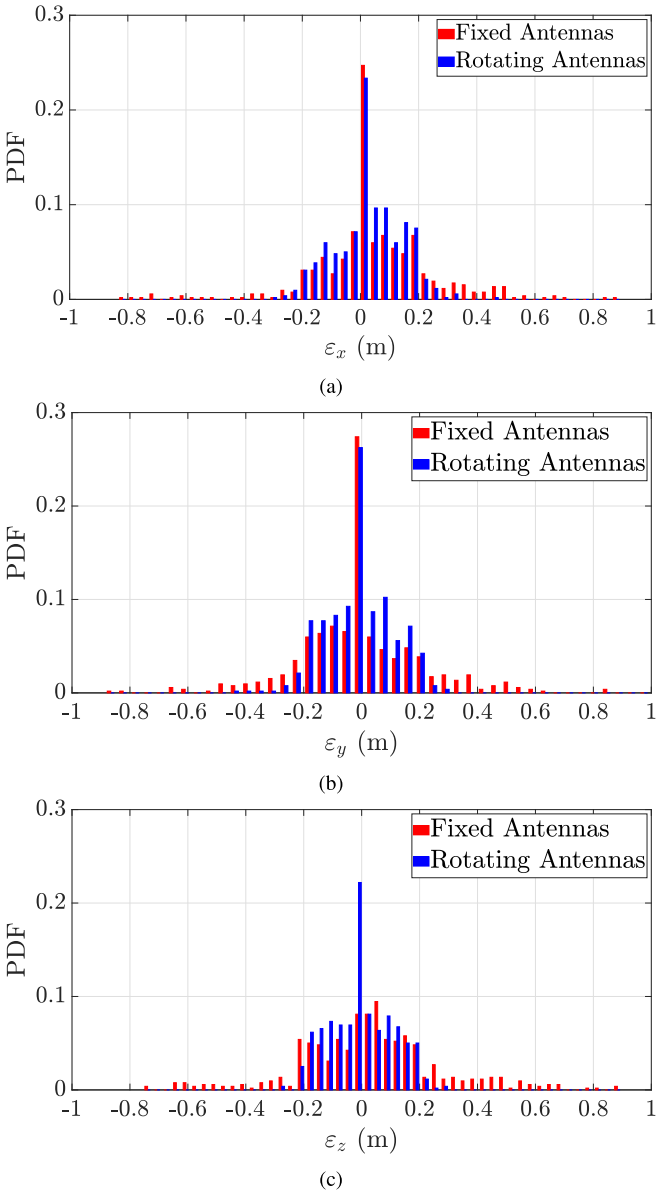

Fig. 13. Histograms of localization errors for fixed antennas (383 tag, red bars), and rotating antennas (565 tags, blue bars) along (a) *X*-axis; (b), *Y*-axis; (c) *Z*-axis. Both shelf tags and clothing tags are included.

configurations. This can be attributed to several factors, *i)* tags attached to clothes are in reduced visibility with respect to antennas on robot and this may lead to a non-uniformly sampled phase-curve with large interval of missed readings (Fig. 10); *ii)* the metallic racks increase the amplitude of multipath contributions; *iii)* the clothing fabrics can affect the tag backscattered signal; *iv)* the mutual coupling among tags is high due to their small distance; *v)* tag orientations on clothes labels is random, by varying the depolarization coefficient with the reader antenna.

The histograms of the localization errors for each coordinate are represented in Fig. 13. A total of 383 tags are considered for the fixed-antennas configuration (red bars), whereas 565 tags were inspected for rotating-antennas one (blue bars). Both shelf tags and clothing tags are included. Mean localization errors along the three axes $\bar{x}$, $\bar{y}$, and $\bar{z}$, and standard

TABLE III
MEAN LOCALIZATION ERRORS AND STANDARD DEVIATIONS FOR FIXED-ANTENNAS AND ROTATING-ANTENNAS CONFIGURATIONS WITH REFERENCE TO THE HISTOGRAMS OF FIG. 13

	$\bar{x}$ (cm)	$\bar{y}$ (cm)	$\bar{z}$ (cm)	s_x (cm)	s_y (cm)	s_z (cm)
Fixed antennas	4.3	<1	3	21	22.5	24
Rotating antennas	2.6	<1	<1	11	11	11

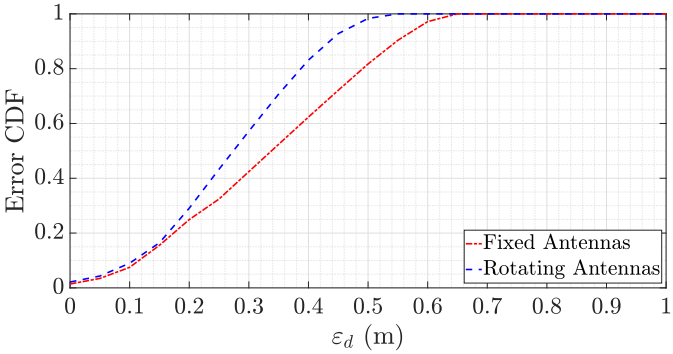

Fig. 14. Cumulative Distribution Function (CDF) of the 3D localization error ε_d for both shelf tags and clothing tags by adopting fixed-antennas configuration (red dash-dotted line) and rotating-antennas (blue dashed line).

deviations s_x, s_y, and s_z are resumed in Table III, as gathered from the histograms. The introduction of the rotating-antenna mechanism on the robot highlights a significant reduction of the localization error along the vertical direction, and also reduces the localization-error standard-deviation thanks to larger synthetic apertures with respect to the robot with fixed antennas.

To evaluate the whole localization performance, the cumulative distribution function (CDF) of the 3D localization error ε_d is shown in Fig. 14 for both shelf tags and clothing tags, by considering the three setups. A total of 383 tag are localized with the fixed-antennas configuration (red line), whereas 565 tags were localized with the rotating-antennas one (blue line). With rotating-antennas configuration, the 3D localization error is bounded to 40 cm in around 85% of cases and it reaches 52 cm as an upper bound. With fixed-antennas configuration the same localization error of 40 cm is reached only in 63% of cases and the upper bound is equal to 64 cm. Finally, a discussion about elaboration and acquisition time should be faced. By assuming the same robot velocity on the plane perpendicular to the floor for both fixed and rotating-antennas configurations, the robot typically takes a few seconds to scan a given shelf. During this timeframe, the rotating antenna system supports a speed allowing for at least a half rotation, maximizing synthetic apertures to their full span, equivalent to the circumference diameter. Consequently, there is no added time required to gather sufficient data for SAR processing with rotating-antennas configuration compared to fixed-antennas one.

V. CONCLUSION

The development and testing of the MONITOR UHF-RFID robot for automated inventory and 3D localization through synthetic aperture-based methods have yielded encouraging results. The incorporation of the antenna rotation mechanism has allowed a highly reliable inventory even for tags in NLOS, moreover, a higher reading rate with respect to the fixed-antennas configuration has been observed, thus improving the probability of tag detection. Besides, the localization accuracy has been notably enhanced thanks to the additional degree of freedom in the antenna motion. The system can work for an arbitrary trajectory of the robot base, which is not constrained to move along a rectilinear trajectory, by allowing more flexibility in the system application.

An experimental analysis has been conducted in a shop-like realistic scenario replicated in an indoor laboratory with high-density tag deployment, by challenging the system under demanding conditions in terms of interference and tag mutual coupling. Tags have been positioned both on card boxes on wooden shelves and on the labels of clothes hung on metal racks, which further contribute to enhance multipath propagation.

The robot navigation system-based on both a depth and a tracking camera has allowed a reliable reconstruction of the antenna position during rotation as essential to apply SAR-based localization. With the aid of the rotating-antennas system, tag inventory has been accomplished with a 100% success rate, and tag mean localization error was in the order of a few-decimeters for both shelf and clothing tags. Effects of clothing fabrics, metallic objects, tag mutual coupling, and NLOS conditions have increased the standard deviation of the tag localization error, which however has been kept bounded to a maximum error of few decimeters, compatible with tagged object sizes.

Obtained performance represents an improvement with respect to current commercial solutions providing item shelf-level or area-level localization. Indeed, the incorporation of antenna rotation mechanisms represents a promising advancement and the MONITOR robot offers a suitable, reliable, scalable, and practical solution for automated inventory and product localization in large stores and warehouses.

Further exploitations will involve alternative solutions for robot navigation that impact tag localization. Improving the knowledge of the robot-antenna trajectory will benefit the tag localization. We will also explore the possibility of using some reference UHF-RFID passive tags to help the robot navigation. On the other hand, to improve tag localization in crowded indoor scenarios, we will consider algorithms suitable for multipath cancellation. Eventually, a refinement on both the instantaneous antenna positioning and the tag localization may pave the way for the development of a robot with rotating arms that can be also equipped with a grasping system for item picking up.

REFERENCES

[1] V. V. Unhelkar et al., "Mobile robots for moving-floor assembly lines: Design, evaluation, and deployment," *IEEE Robot. Autom. Mag.*, vol. 25, no. 2, pp. 72–81, Jun. 2018.

[2] M. B. Alatise and G. P. Hancke, "A review on challenges of autonomous mobile robot and sensor fusion methods," *IEEE Access*, vol. 8, pp. 39830–39846, 2020.

[3] K. Sakai, Y. Nakamura, Y. Yoshikawa, and H. Ishiguro, "Effect of robot embodiment on satisfaction with recommendations in shopping malls," *IEEE Robot. Autom. Lett.*, vol. 7, no. 1, pp. 366–372, Jan. 2022.

[4] F. Zafari, A. Gkelias, and K. K. Leung, "A survey of indoor localization systems and technologies," *IEEE Commun. Surveys Tuts.*, vol. 21, no. 3, pp. 2568–2599, 3rd Quart., 2019.

[5] P. Tripicchio, M. Unetti, N. Giordani, C. A. Avizzano, and M. Satler, "A lightweight slam algorithm for indoor autonomous navigation," in *Proc. Australas. Conf. Robot. Autom. (ACRA)*, 2014, pp. 2–4.

[6] G. Pepe, M. Satler, and P. Tripicchio, "Autonomous exploration of indoor environments with a micro-aerial vehicle," in *Proc. Workshop Res., Educ. Develop. Unmanned Aerial Syst. (RED-UAS)*, 2015, pp. 43–52.

[7] P. Tripicchio, M. Satler, C. Avizzano, and M. Bergamasco, "Autonomous navigation of mobile robots: From basic sensing to problem solving," in *Proc. 20th IMEKO TC4 Int. Symp. 18th Int. Workshop ADC Model. Test. Res. Elect. Electron. Meas. Econ. Upturn*, 2014, pp. 15–17.

[8] M. R. U. Saputra, A. Markham, and N. Trigoni, "Visual SLAM and structure from motion in dynamic environments: A survey," *ACM Comput. Surv.*, vol. 51, no. 2, pp. 1–36, 2018.

[9] Z. Zou, Z. Shi, Y. Guo, and J. Ye, "Object detection in 20 years: A survey," 2019, *arXiv:1905.05055*.

[10] Y.-T. Wang, C.-C. Peng, A. A. Ravankar, and A. Ravankar, "A single LiDAR-based feature fusion indoor localization algorithm," *Sensors*, vol. 18, no. 4, p. 1294, 2018.

[11] P. Tripicchio, M. Satler, M. Unetti, and C. A. Avizzano, "Confined spaces industrial inspection with micro aerial vehicles and laser range finder localization," *Int. J. Micro Air Veh.*, vol. 10, no. 2, pp. 207–224, 2018.

[12] A. Motroni, F. Bernardini, A. Buffi, P. Nepa, and B. Tellini, "A UHF-RFID multi-antenna sensor fusion enables item and robot localization," *IEEE J. Radio Freq. Identif.*, vol. 6, pp. 456–466, Apr. 2022.

[13] A. Motroni, A. Buffi, and P. Nepa, "Forklift tracking: Industry 4.0 implementation in large-scale warehouses through UWB sensor fusion," *Appl. Sci.*, vol. 11, no. 22, Nov. 2021, Art. no. 10607.

[14] A. Motroni, P. Nepa, A. Buffi, P. Tripicchio, and M. Unetti, "RFID tag localization with UGV in retail applications," in *Proc. 3rd Int. Conf. Smart Sustain. Technol. (SpliTech)*, 2018, pp. 1–5.

[15] A. Motroni and A. Buffi, "RFID robots and vehicles for item inventory and Localization," in *Proc. 17th Eur. Conf. Antennas Propagat. (EuCAP)*, 2023, pp. 1–5.

[16] V. Casamayor-Pujol, B. Gastón, S. López-Soriano, A. A. Alajami, and R. Pous, "A simple solution to locate groups of items in large retail stores using an RFID robot," *IEEE Trans. Ind. Informat.*, vol. 18, no. 2, pp. 767–775, Feb. 2022.

[17] M. Gareis, A. Parr, J. Trabert, T. Mehner, M. Vossiek, and C. Carlowitz, "Stocktaking robots, automatic inventory, and 3D product maps: The smart warehouse enabled by UHF-RFID synthetic aperture localization techniques," *IEEE Microw. Mag.*, vol. 22, no. 3, pp. 57–68, Mar. 2021.

[18] F. Bernardini et al., "Robot-based indoor positioning of UHF-RFID tags: The SAR method with multiple trajectories," *IEEE Trans. Instrum. Meas.*, vol. 70, 2021, Art. no. 8001415.

[19] A. Tzitzis et al., "Localization of RFID tags by a moving robot, via phase unwrapping and non-linear optimization," *IEEE J. Radio Freq. Identif.*, vol. 3, no. 4, pp. 216–226, Dec. 2019.

[20] P. Tripicchio et al., "A synthetic aperture UHF RFID localization method by phase unwrapping and hyperbolic intersection," *IEEE Trans. Autom. Sci. Eng.*, vol. 19, no. 2, pp. 933–945, Apr. 2022.

[21] F. Ali, G. Bauer, and M. Vossiek, "A rotating synthetic aperture radar imaging concept for robot navigation," *IEEE Trans. Microw. Theory Tech.*, vol. 62, no. 7, pp. 1545–1553, Jul. 2014.

[22] R. Bogue, "Strong prospects for robots in retail," *Ind. Robot*, vol. 46, no. 3, pp. 326–331, Jan. 2019.

[23] "xArray gateway product brief / Datasheet," Data sheet, Impinj Radio-Freq. Identif. Co., Seattle, WA, USA, 2023. [Online]. Available: https://support.impinj.com/hc/en-us/articles/202755688-xArray-Gateway-Product-Brief-Datasheet

[24] F. Bernardini, A. Motroni, P. Nepa, P. Tripicchio, A. Buffi, and L. Del Col, "The MONITOR project: RFID-based robots enabling real-time inventory and localization in warehouses and retail areas," in *Proc. 6th Int. Conf. Smart Sustain. Technol. (SpliTech)*, 2021, pp. 1–6.

[25] F. Bernardini et al., "Retail robots with UHF-RFID moving antennas enabling 3D localization," in *Proc. IEEE 12th Int. Conf. RFID Technol. Appl. (RFID-TA)*, 2022, pp. 1–4.

[26] P. Nepa, F. Lombardini, and A. Buffi, "Method for determining the location of a moving RFID tag," European Patent 2 533 173 B1, 2011.

[27] A. Buffi, P. Nepa, and F. Lombardini, "A phase-based technique for localization of UHF-RFID tags moving on a conveyor belt: Performance analysis and test-case measurements," *IEEE Sensors J.*, vol. 15, no. 1, pp. 387–396, Jan. 2015.

[28] G. Cecchi et al., "The MONITOR robot with UHF-RFID rotating antennas enhancing indoor tag Localization," in *Proc. 8th Int. Conf. Smart Sustain. Technol. (SpliTech)*, 2023, pp. 1–6.

[29] A. Motroni, A. Buffi, and P. Nepa, "UHF-RFID SAR robotic inventory and localization: Handling systems vs. multi-antenna solutions," in *Proc. IEEE Int. Conf. RFID (RFID)*, 2022, pp. 138–143.

[30] A. A. Alajami, G. Moreno, and R. Pous, "A ROS gazebo plugin design to simulate RFID systems," *IEEE Access*, vol. 10, pp. 93921–93932, 2022.

[31] S. D'Avella, M. Unetti, and P. Tripicchio, "RFID gazebo-based simulator with RSSI and phase signals for UHF tags localization and tracking," *IEEE Access*, vol. 10, pp. 22150–22160, 2022.

[32] M. Labbé and F. Michaud, "RTAB-map as an open-source lidar and visual simultaneous localization and mapping library for large-scale and long-term online operation," *J. Field Robot.*, vol. 36, no. 2, pp. 416–446, 2019.

[33] D. Scaramuzza and F. Fraundorfer, "Visual odometry [tutorial]," *IEEE Robot. Autom. Mag.*, vol. 18, no. 4, pp. 80–92, Dec. 2011.

[34] D. Fox, W. Burgard, F. Dellaert, and S. Thrun, "Monte carlo localization: Efficient position estimation for mobile robots," in *Proc. AAAI/IAAI*, 1999, pp. 2–2.

[35] J. Sturm, N. Engelhard, F. Endres, W. Burgard, and D. Cremers, "A benchmark for the evaluation of RGB-D SLAM systems," in *Proc. IEEE/RSJ Int. Conf. Intell. Robots Syst.*, 2012, pp. 573–580.

[36] F. Bernardini et al., "Particle swarm optimization in SAR-based method enabling real-time 3D positioning of UHF-RFID tags," *IEEE J. Radio Freq. Identif.*, vol. 4, no. 4, pp. 300–313, Dec. 2020.

Andrea Motroni (Member, IEEE) received the M.E. degree (with Hons.) in telecommunication engineering and the Ph.D. degree (with Hons.) in information engineering from the University of Pisa, Pisa, Italy, in 2017 and 2021, respectively, where he is currently an Assistant Professor. In 2019, he was the President of the IEEE Student Branch of the University of Pisa. In 2020, he was a visiting Ph.D. student with the Graz University of Technology, Graz, Austria. His current research interests include indoor radiolocalization systems, with specific focus on UHF-RFID and UWB technology for robot and vehicle localization, the integration of robotic systems with RFID towards new systems for industry and logistics, UHF-RFID smart gates and other RFID-based applications for Internet of Things, Industry 4.0, and people safety in both indoor and outdoor environments. He was a recipient of the Best Paper Award and Best Student Paper Award at IEEE RFID-TA 2019, and a recipient of the Young Scientist Award from the International Union of Radio Science, Commission B, in 2018, 2019, and 2021, respectively. In 2022, he was awarded with the IEEE/ABB Italy Section Award for Ph.D. Thesis. In 2022, he was also awarded with the "2021 Best Ph.D. Dissertation in the field of Information and Industrial Engineering" from the University of Pisa and the "Best Poster Award" at IEEE M&N 2022. In 2023, he was again recognized with Young Scientist Award from the International Union of Radio Science, Commission B, and with "Best Poster Award" at IEEE RFID 2023. He was a Finalist at the IEEE CRFID Educational Mega Challenge. He currently serves as an Associate Editor for the IEEE JOURNAL OF RADIO FREQUENCY IDENTIFICATION. He has joined the Organizing Committee and has been Session Chair of several IEEE international conferences. He is an Executive Member of the IEEE CRFID's Technical Committee on Motion Capture and Localization.

Salvatore D'Avella (Member, IEEE) received the bachelor's degree (with Hons.) in computer engineering from the University of Pisa, the master's degree (with Hons.) in embedded computer systems from the Sant'Anna School of Advanced Studies, and the Ph.D. degree (with Hons.) in perceptual robotics from the Department of Excellence in Robotics & AI, Sant'Anna School of Advanced Studies. He is an Assistant Professor with the Department of Excellence in Robotics and Artificial Intelligence, Institute of Mechanical Intelligence, Scuola Superiore Sant'Anna. He was a visiting Ph.D. student with the Institute of Robotics and Mechatronics (DLR), Munich, Germany. His main research areas are computer vision, artificial intelligence, and robotics, applied to industry 4.0, and logistics. He has been an Associate Editor of the 16th IEEE/SICE International Symposium on System Integration and 2024 IEEE International Conference on Robotics and Automation conferences. He is also an Associate Editor for the IEEE ROBOTICS AND AUTOMATION LETTERS. He has been the session chair and the co-chair of many international conferences.

Alice Buffi (Senior Member, IEEE) received the B.S. and M.S. degrees (summa cum laude) in telecommunications engineering and the Ph.D. degree (Doctor Europaeus) in applied electromagnetism in electrical and biomedical engineering, electronics, smart sensors, nanotechnologies from the University of Pisa, Pisa, Italy, in 2006, 2008 and 2012, respectively. Since 2012, she has been with the University of Pisa, where she is currently an Associate Professor with the Department of Energy, Systems, Territory and Construction Engineering. Her current research topics include measurement methods to locate static or moving items through RFID systems operating at the UHF band in Industry 4.0 scenarios. Besides, she has interests in classification methods for smart gates and smart storage systems and aging process in battery cells. She was a recipient of the Best Paper Award at the 2019 IEEE International Conference RFID-TA, the Best Poster Award at the 2022 IEEE International Symposium on Measurements and Networking, the Best Poster Award at the 2023 IEEE International Conference RFID, and of the Young Scientist Award from the International Union of Radio Science, Commission B, in 2013 and 2016. She was also a recipient of the recognition as "2022 IEEE Open Journal of Instrumentation and Measurement Outstanding Reviewer" by the Instrumentation and Measurement Society. She serves as the VP of Publications of the IEEE CRFID. She serves as an Associate Editor for the IEEE TRANSACTIONS ON INSTRUMENTATION AND MEASUREMENT and the IEEE JOURNAL OF RADIO FREQUENCY IDENTIFICATION. She also serves as the Steering Committee Chair of the IEEE JOURNAL OF RADIO FREQUENCY IDENTIFICATION and as the Chair of the IEEE CRFID's Technical Committee on Motion Capture and Localization. Moreover, she serves as a Distinguished Lecturer of the IEEE Council of RFID from 2023 to 2025.

Paolo Tripicchio (Senior Member, IEEE) received the master's degree in automation engineering from the University of Pisa, and the Ph.D. degree (cum laude) in perceptual robotics from the Sant'Anna School of Superior Studies, Pisa, Italy, in 2012, where he is an Assistant Professor with the Department of Excellence in Robotics and AI, Mechanical Intelligence Institute. In 2012, he was an Invited Lecturer with the Orizaba Institute of Technology, Mexico, teaching classes on virtual reality and its applications. In 2016, he taught computer vision for autonomous drones with the Autonomous University of Toluca, Mexico. Since January 2013, he has been the Scientific Program Manager with the Gustavo Stefanini Advanced Robotics Research Center, La Spezia, Italy, dedicated to the advancements in mobile and field robotics. His main research areas cover different technological topics, such as studies on robotic perception, applications and theories of computer vision, AI systems and their applications, human-machine interaction with a particular focus on haptics, the fast-growing industrial robotics sector, field robotics applications, and the use of virtual and augmented reality for visualization, interaction, and simulation. He was the recipient of the Best Paper Award at the International Conference on Systems, Analysis and Automatic Control of the 11th International Multi-Conference on Systems, Signals and Devices 2014, the Best Paper Award Finalist at the 2019 IEEE International Conference on Real-time Computing and Robotics, the One Star Innovation Award at MBDA Innovation Awards 2020, and of the 2020 Researcher prize in Artificial Intelligence from the Department of Excellence in Robotics and AI of the Scuola Superiore Sant'Anna.

Matteo Unetti received the M.Sc. degree in automation engineering from the University of Pisa in 2003. He is currently a Research Fellow with the Gustavo Stefanini Advanced Robotics Research Center, a joint research center between Scuola Superiore Sant'Anna and Leonardo company (formerly Finmeccanica) on mobile robots. His research activity concerns robotics, sensor fusion, localization, computer vision, and control systems.

Glauco Cecchi (Student Member, IEEE) received the M.E. degree in telecommunication engineering from the University of Pisa, Pisa, Italy, in 2020, where he is currently pursuing the Ph.D. degree (Smart Industry) with the Department of Information Engineering, Microwave Research Lab. His research is about passive radio frequency identification systems application in Industry 4.0.: he is focusing on applying this technology for the inventory management operations and for radiolocalization in indoor environments.

Paolo Nepa (Senior Member, IEEE) received the Laurea degree (summa cum laude) in electronics engineering from the University of Pisa, Pisa, Italy, in 1990. Since 1990, he has been with the Department of Information Engineering, University of Pisa, where he is currently a Full Professor. He is also affiliated with the Institute of Electronics, Computer and Telecommunication Engineering, Italian National Research Council, Turin, Italy. In 1998, he was a Visiting Scholar with the Electro Science Laboratory (ESL), The Ohio State University, Columbus, OH, USA, supported by a grant from the Italian National Research Council. At ESL, he was involved in research on efficient hybrid techniques for the analysis of large antenna arrays. He has coauthored more than 300 international journal articles and conference contributions. His research interests are in the design of wideband and multiband antennas for mobile communication systems and antennas optimized for near-field coupling and focusing, as well as in the development of propagation models of wireless radio links for indoor and outdoor scenarios. He is also working on channel characterization, wearable antenna design, and diversity scheme implementation for body-centric communication systems. In the context of UHF-RFID systems, he is working on efficient and accurate techniques for radio localization of either tagged static objects or vehicles, in the Internet of Things and Industry4.0 scenarios. He was a recipient of the Young Scientist Award from the International Union of Radio Science, Commission B, in 1998. He was a recipient of the Outstanding Associate Editors Awards in 2021. Since October 2016 until 2022, he has served as an Associate Editor for the IEEE ANTENNAS AND WIRELESS PROPAGATION LETTERS. In 2019, he has served as the General Chair for the IEEE RFID-TA 2019, Pisa, from 25–27 September 2019. Since 2021, he has been serving as an Associate Editor for the IEEE TRANSACTIONS ON ANTENNAS AND PROPAGATION. Since 2023, he has been serving as the Editor in Chief of the IEEE JOURNAL OF RADIO FREQUENCY IDENTIFICATION. Since 2013, he has been a member of the Technical Advisory Board of URSI Commission B—Fields and Waves. He has served as a TPC member of several IEEE international conferences.

Open Access funding provided by 'Università di Pisa' within the CRUI CARE Agreement